Egyptian Journal of Radiology and Nuclear Medicine

RESEARCH

Open Access

Evaluation of the impact of magnetic field homogeneity on image quality in magnetic resonance imaging: a baseline quantitative study at 1.5 T

Eric Naab Manson[1,2*], Abdul Nashirudeen Mumuni[1], Stephen Inkoom[2,3] and Issahaku Shirazu[2,4]

Abstract

Background Magnetic resonance images can be affected in a number of ways by magnetic field inhomogeneity. The study aimed to optimize the main magnetic field homogeneity (MFH) by assessing how magnetic field inhomogeneity affects the signal-to-noise ratio (SNR) and geometric distortion of images acquired along the diameter of a spherical volume phantom from the isocenter of the MRI scanner.

Results The MFH ranged between 0.10 and 0.60 ppm. The best MFH and the maximum SNR were determined in the isocenter at 400 mm field of view with the application of shim. However, for all the phantom positions, geometrical distortion in images acquired at 200 mm field of view was generally better and worse at 400 mm field of view. MFH could be optimized to reduce geometrical distortion and increase SNR by increasing the receiver bandwidth and the number of excitations whiles complementing it with shimming during image acquisition. According to Chi-square independent test, there were no significant differences ($p > 0.05$) in the MFH, SNR, and geometrical distortion values. Compared to findings at higher field strengths, it was observed that MRI systems of higher field strengths (greater than 1.5 T) could offer superior magnetic field homogeneity and SNR without causing observable geometrical distortion.

Conclusions The optimal field of view for the fast field echo (FFE) sequence required to maximize MFH, SNR, and reduce distortion during image acquisition may vary across MRI systems of different field strengths. To determine the appropriate field of view, the method and results of this study could serve as a guide for medical physicists as part of their routine quality assurance test procedures.

Keywords Bandwidth difference, Magnetic field homogeneity, Geometrical distortion, Signal-to-noise ratio, MRI quality control

*Correspondence:
Eric Naab Manson
emanson@uds.edu.gh
Full list of author information is available at the end of the article

Background

Fast field echo (FFE) also known as gradient echo is a magnetic resonance (MR) pulse sequence widely employed in the acquisition of MR images, especially in applications such as cardiac magnetic resonance imaging (MRI) and contrast-enhanced MR angiography [1]. FFE imaging reduces both imaging time and motion artifacts and is useful for evaluating critically ill, anxious, or reluctant patients [2]. The magnetic field generated by an MRI scanner at the isocenter or magnet's center is highly homogeneous. Away from the isocenter (i.e., towards the edges of the magnet), the magnetic field homogeneity decreases which could affect the quality of the images that are produced. This phenomenon occurs more frequently in investigations that involve large fields of view (FOV) when FFE sequences are employed [3]. The variations in tissue magnetic susceptibility also contribute to the main magnetic field's (B_0) inhomogeneities [4]. Because of these effects, FFE sequences are not frequently used in brain imaging [5].

The challenge of establishing homogeneous excitation and homogeneous signal reception across large fields of view (FOV), particularly across torso anatomy (which cannot be completely encircled by a small birdcage transmit coil), is a significant limitation for musculoskeletal imaging at high field strength [6]. Even if it would be possible to position the patient so that the body component being scanned is at the isocenter, some positions can be uncomfortable and painful, resulting in motion artifacts, extended acquisition periods, or repeated scanning [3]. Also, at low field strengths, inhomogeneities can decrease image signal uniformity, increase wrap artifacts, compromise signal-to-noise ratio (SNR) and cause geometrical distortion [7].

The geometrical distortion and loss in SNR in the FFE sequence are due to the effect of magnetic field inhomogeneity at the Larmor frequency of the hydrogen nuclei [8–10]. Geometric distortions in MRI are frequently minimal. As a result, they are generally disregarded in diagnostic procedures. However, distortions could affect image geometry procedures such as the planning of tangential whole breast intensity-modulated radiation and stereotactic radiosurgery. Reducing geometric distortions may help improve treatment outcomes by lowering the overall inaccuracy in these image geometry processes [11].

Some of the well-established techniques used to measure magnetic field homogeneity (MFH) include bandwidth difference (ΔBW), resonance frequency mapping, full width at half maximum (FWHM), and phase shift mapping methods [9]. The ΔBW approach takes advantage of the dependence of spatial distortion on gradient strength and field homogeneity to estimate MFH by comparing the spatial distortion observed at the same FOV for both low and high bandwidths in the frequency-encoding direction [7]. The bandwidth difference method has the benefit of allowing for the measurement of various diameters of spherical volumes in a single phantom. It is more practical and typically more adaptable to routine clinical MRI performance evaluations. Additionally, the technique has been tried on seven distinct clinical MRI system models, with consistent outcomes [9].

Chen et al. [9] investigated the accuracy of the bandwidth difference method for evaluating magnetic field homogeneity (MFH) by comparing it with the full width at half maximum (FWHM) and phase difference method. In another study, Jang et al. [12] compared SNR and geometrical distortion between a 3 T conventional and wide-bore MRI system. However, both studies were conducted with a single FOV. Also, the influence of MFH on image quality was not discussed. This paper aims to optimize magnetic field homogeneity resulting from the fast field echo (FFE) pulse sequence on a 1.5 T MRI scanner using a spherical quality control phantom. To achieve this aim, we evaluated how changes in FOV and phantom positions from the isocenter could influence MFH measurements on geometrical distortion (GD) and signal-to-noise ratio (SNR) using the bandwidth difference technique.

Methods

The phantom used for this study was spherical of 15 cm diameter containing 0.019 M Nickel Chloride solution in 1.44 L of water, manufactured and supplied by the manufacturer of the MRI system (Philips, Amsterdam, Netherlands). Spherical phantoms are ideal for evaluating the homogeneity of the B_0 field because they can be maintained at a constant position within the magnetic bore for each plane (i.e., axial, sagittal, and coronal) without any rotation [4].

On the MRI couch, the anterior body coil was placed over the phantom near the bore of the magnet (Fig. 1) and padded to the isocenter. Using a matrix size of 256×256 for different FOVs and setting the bandwidth to the lowest value, the first scan was performed in the axial plane while keeping the sequence parameters constant in the frequency-encoding direction. This was followed with a second scan in the same plane using the highest bandwidth value. The procedure was repeated in the sagittal and coronal planes. There was no table motion during the low and high bandwidth scans in each of the three planes. The entire procedure was then repeated for different phantom positions (i.e., 20, 40, 60, 40, 60 and 80 mm) from the isocenter. After the scans were completed, the diameter of the image sphere was measured and recorded in millimeters. The MFH was then calculated from Eq. 1

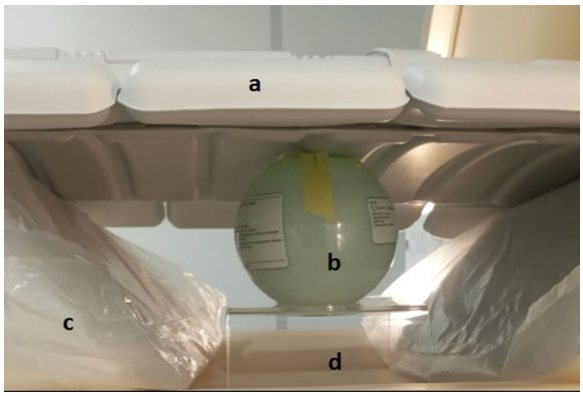

Fig. 1 Phantom placed at the center of the anterior coil. (a) anterior coil, (b) spherical phantom, (c) support, (d) phantom stand

Table 1 Image acquisition parameters used for the bandwidth magtic field homogeneity measurements

Parameter	Description
Sequence type	FFE
TR	50 ms
TE	9 ms
Flip angle	25°
FOV	200, 250, 300, 350, 400 mm
Acquired voxel size	0.78/0.78/6.00 mm
Acquisition matrix	256 × 256
Number of slices	23
Scan time	1 min:06 s
NEXT	1
Slice thickness	5 mm
BW_1	10.95 kHz
BW_2	88.00 kHz

FFE, Fast field echo; NEXT, Number of excitations; FOV, Field of view; BW_1, low bandwidth value; BW_2, high bandwidth value

[9]. The sequence parameters utilized for the scan are shown in Table 1.

$$MFH_{(ppm)} = \frac{BW_1 * BW_2 * (x_1 - x_2)}{¥B_o * FOV * (BW_2 - BW_1)} \quad (1)$$

$$¥ = \frac{\gamma}{2\pi} \quad (2)$$

where BW_1 = low bandwidth in Hz, BW_2 = high bandwidth in Hz, $(x_1 - x_2)$ = diameter of sphere in mm, $¥B_o$ = center of frequency in MHz, FOV = field of view in mm, γ = gyromagnetic ratio.

In order to investigate the influence of MFH on image quality for each phantom position, the SNR and geometrical distortion were determined according to the method described in ACR Report 2015 [7] and AAPM Report 100 [13]. For the SNR measurement and using the RadiAnt DICOM viewer (64-bit), the mean signal intensity and standard deviation from the region of interest in elliptical shapes with a roughly 50 cm^2 area were acquired. Also, the distance tool was used to estimate the phantom image's internal and external diameters. To evaluate image SNR and geometrical distortion, the results from each slice for the different phantom positions and their related FOVs were compared. Equations 3 and 4 were used to calculate the SNR and geometrical distortion respectively.

$$SNR = \frac{(\bar{I})}{\sigma_{bn}} \quad (3)$$

$$GD = \frac{|l_d - l_x|}{l_x} \quad (4)$$

where $\bar{I}$ is the mean signal intensity from the ROI containing 75% of the phantom area, σ_{bn} is the standard deviation of the measured signal intensity, l_x is the external diameter of the phantom image and l_d is the internal diameter of the phantom image.

The data analysis was performed using the Statistical Package for the Social Sciences (SPSS) software (version 20, IBM Corp., USA). The Chi-square test for independence was utilized to examine whether a significant relationship existed between magnetic field homogeneity (with and without active shimming), signal-to-noise ratio and, geometrical distortion. Statistical significance was set at alpha value of $p < 0.05$.

Results

The images for MFH measurements from the spherical $NiCl_2$ homogeneous phantom for both high and low bandwidths in the frequency-encoding direction are shown in Fig. 2. The image representing SNR measurement is shown in Fig. 3. Measurement of internal and external diameters of the phantom image is also shown in Fig. 4. From the high bandwidth images, the isocenter location at 400 mm FOV had the highest mean signal intensity, whereas the 60 mm phantom position from the isocenter had the lowest mean signal intensity.

Additionally, for the images acquired with the smaller bandwidth, the maximum mean signal strength was discovered at 400 mm FOV and 40 mm from the isocenter while the lowest mean signal intensity at the same phantom position was recorded at 200 mm FOV. Although the lowest mean signal intensity was recorded at 200 mm FOV, the magnetic field uniformity was found to be better across all the phantom positions investigated

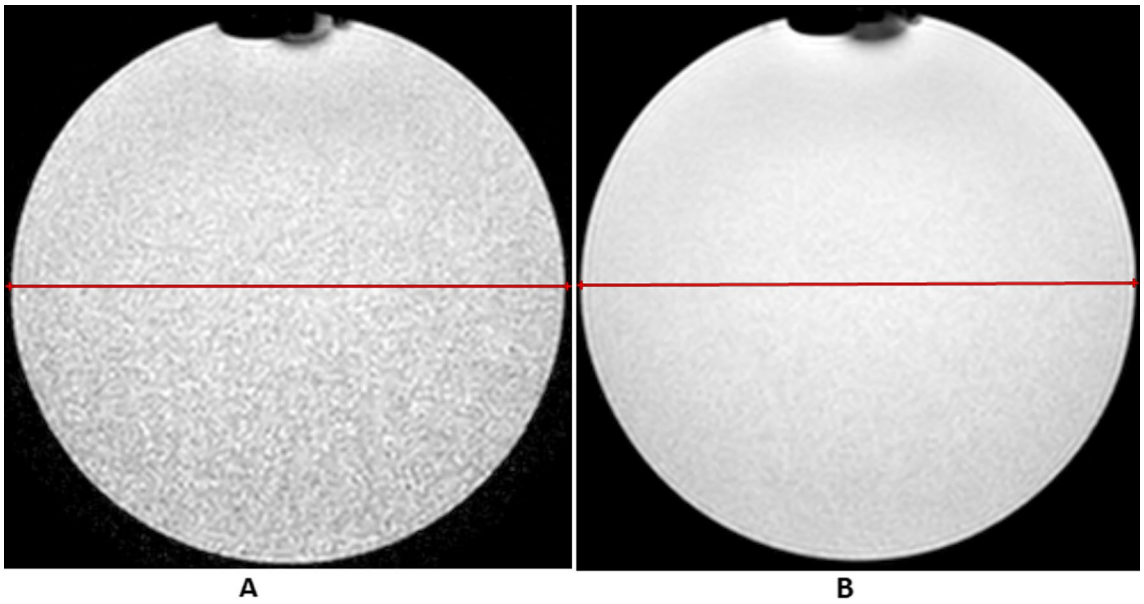

Fig. 2 Measurement of MFH in the frequency-encoding direction using the bandwidth difference method. **A** Diameter of axial image of the phantom acquired with low bandwidth. **B** Diameter of axial image of the phantom acquired with high bandwidth

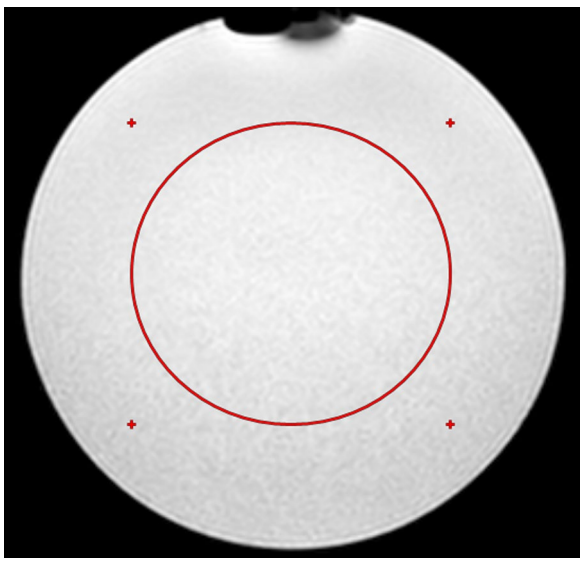

Fig. 3 Measurement of SNR with high bandwidth. Mean signal intensity measured at isocenter using a ROI of approximately 50 cm^2 in area

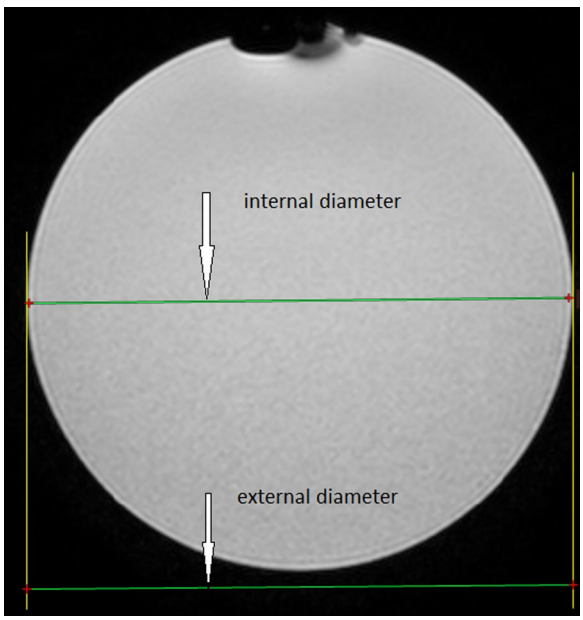

Fig. 4 Geometrical distortion measurement from internal and external diameter of the phantom image

(0.40 ≤ MFH ≤ 0.60 ppm) with and without the application of shim at 200 mm FOV except at the 400 mm FOV which had the best uniformity (0.10 ≤ MFH ≤ 0.56 ppm).

As the phantom position was increased from the isocenter, the homogeneity of the magnetic field worsened; the FOV was also increased until a sharp improvement in MFH was achieved at a FOV of 400 mm. The variation of MFH with phantom positions at various FOVs without and with the application of shim is shown in Figs. 5 and 6 respectively. There was no particular variation observed with geometrical distortion and SNR measured for both high and low

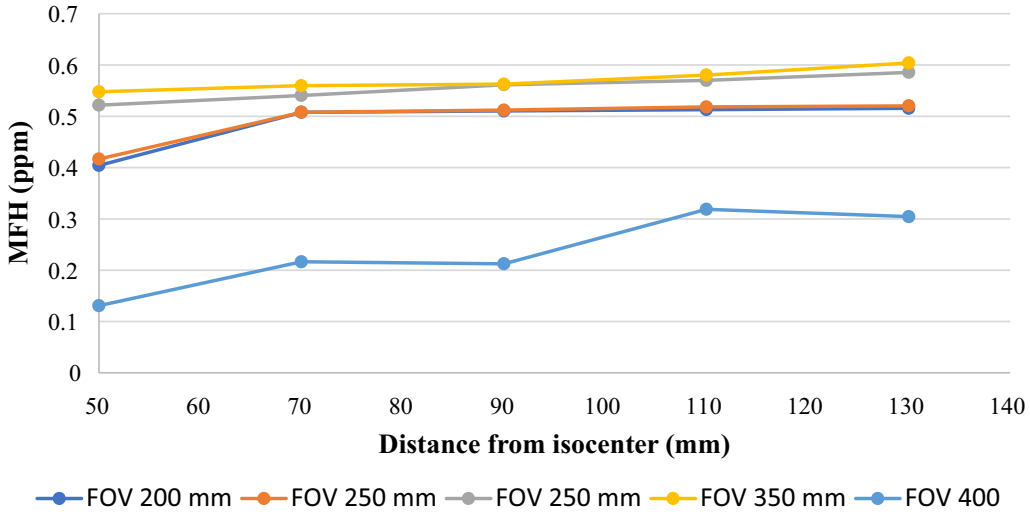

Fig. 5 MFH at different phantom positions for various FOVs without the application of shim

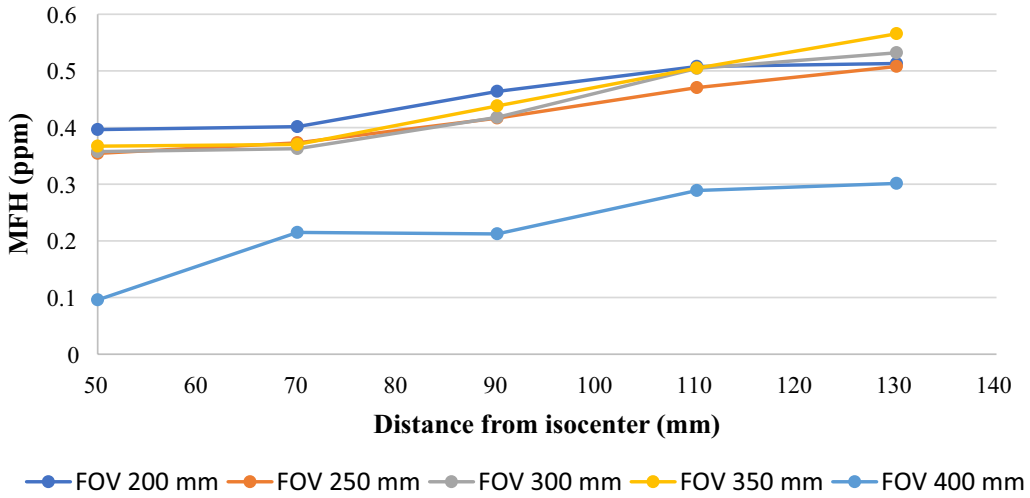

Fig. 6 MFH at different phantom positions for various FOVs with the application of shim

Table 2 SNR measurements at different FOVs and phantom positions for high bandwidth (HBW) and low bandwidth (LBW)

Position (mm)	FOV at HBW (mm)					FOV at LBW (mm)				
	200	250	300	350	400	200	250	300	350	400
Isocenter	31.98	37.98	39.6	42.72	43.06	12.44	17.85	22.74	27.48	31.55
20	30.79	36.45	37.2	37.52	37.98	12.99	17.44	22.63	27	31.27
40	29.69	37.7	40.59	40.92	41.14	12.32	16.55	23.03	27.49	32.71
60	28.52	33.17	38.06	34.52	36.25	12.73	17.19	22.76	26.47	30.97
80	31.26	34.69	35.82	36.94	35.62	13.97	19.72	25.19	28.57	31.54

bandwidths as the phantom position were changed. However, it is obvious from Tables 2 and 3 that as FOV increased, the SNR and geometrical distortion also increased.

No statistical differences were observed in the MFH values between with and without the application of shimming as the phantom positions and FOV were varied. Likewise, as the field of views (FOVs) and phantom

Table 3 Geometrical distortion (GD) measurements at different FOVs and phantom positions for high bandwidth (HBW) and low bandwidth (LBW)

Position (mm)	GD (%) ± 0.10 at HBW					GD (%) ± 0.13 at LBW				
	200	250	300	350	400	200	250	300	350	400
Isocenter	0.28	0.30	0.31	0.33	0.41	0.29	0.30	0.35	0.41	0.58
20	0.28	0.37	0.42	0.42	0.48	0.33	0.35	0.48	0.49	0.57
40	0.24	0.28	0.30	0.41	0.46	0.30	0.34	0.42	0.66	0.67
60	0.26	0.35	0.36	0.37	0.40	0.37	0.48	0.49	0.49	0.56
80	0.10	0.25	0.35	0.46	0.67	0.14	0.47	0.50	0.66	0.67

positions were varied, no statistically significant difference was found in the signal-to-noise ratio (SNR) values ($p=0.24$) and geometrical distortion values ($p=0.27$) between the high and low bandwidths.

Discussion

In MRI, direct comparisons amongst MRI vendor specifications are somewhat complicated due to the different ways that MFH values are specified. For instance, throughout a range of DSV values, some suppliers report MFH using spectral peak-to-peak while others report in volume root-mean-square (VRMS) metrics. Depending on the manufacturer's requirements for image quality and the available DSVs, usable DSVs often range from 16 to 49 cm. When a 40 cm DSV is used on 1.5 T systems, the B_0 homogeneity varies between 0.35 and 5 ppm, and between 0.2 and 1.4 ppm on 3 T systems [4]. Also, the B_0 inhomogeneity over a 35 cm DSV in current cylindrical superconducting magnets used for routine imaging should not exceed 0.5 ppm and 0.1 ppm for ultrafast imaging or spectroscopy applications [13].

In this study, the magnetic field homogeneity (MFH) was observed to range between 0.6 and 1.3 ppm. When active shimming was applied at all field-of-view (FOV) settings and phantom positions up to 60 mm from the isocenter, the estimated MFH values fell within the range of 0.10 to 0.50 ppm, consistent with findings by Jackson et al. [13]. However, without the use of active shimming, all MFH values, except for those acquired with a 400 mm FOV at all phantom positions and 200–250 mm at the isocenter (ranging from 0.51 to 0.60 ppm), were calculated to be above 0.5 ppm. Although no statistically significant difference ($p=0.13$) in MFH values was observed between active shimming and no shimming, the magnetic field appeared more uniform when shimming was applied.

In larger FOV settings, shimming may be less effective due to increased susceptibility variations and larger field volumes. It should be noted that MFH measurements beyond 80 cm from the isocenter for FOVs above 400 mm were not possible in this study because part of the phantom appeared to cut off from the image. Nevertheless, the MFH values measured above 0.5 ppm are consistent with findings reported by Gach et al. [14]. The higher MFH values (above 0.5 ppm) measured away from the isocenter can be attributed to the smaller size of the phantom DSV (15 cm) used in this study. According to Sandgren [15], phantom volumes smaller than 24 cm may not be sufficient for evaluating the homogeneity of whole-body scanners and might not adequately identify insufficient magnetic field homogeneity [15].

Based on a study conducted by Chen et al. [9], the magnetic field homogeneity (MFH) on a 1.5 T Philips MRI scanner, measured using the bandwidth difference method, varied from 0.8 to 1.3 ppm for a range of DSV sizes from 13 to 22.6 cm. The smaller DSV (13 cm) showed a worse MFH value of 1.3 ppm compared to the larger DSV (22.6 cm) that measured a MFH value of 0.8 ppm [9]. A small DSV phantom may not cover a sufficient volume of the MRI scanner's imaging space. This limited coverage could lead to an incomplete assessment of the magnetic field homogeneity across the entire imaging region. Inhomogeneities outside the small phantom's volume may go undetected, potentially affecting image quality and diagnostic accuracy for clinical exams that extend beyond the phantom's boundaries.

In this current study, using a 15 cm DSV at the same field strength, the MFH values ranged from 0.13 to 0.6 ppm, which were relatively better than the values reported by Chen et al. [9]. This suggests that using a DSV greater than 22.6 cm could have further reduced the MFH values in the current study. A lower ppm value indicates better field uniformity, which is essential for obtaining high-quality images and precise diagnostic information. Possible factors contributing to the improved MFH values in the current study may be attributed to technological advancements and improvements in MRI systems over time, as well as the pulse sequence parameters employed in this study.

Magnetic field inhomogeneities often result from coil winding inaccuracies, external ferromagnetic objects' disturbances [16], and tissues with high magnetic susceptibility [17]. These inhomogeneities cause several artifacts in MR images, leading to spatial distortion, visual blurring, and reduced signal intensity. For example, tissues with varying magnetic susceptibilities, such as air-tissue interfaces, can cause susceptibility artifacts. These artifacts can lead to signal loss and geometric distortions in the images, impacting the accuracy of measurements and anatomical localization. Consequently, the usefulness of MRI scans may be limited due to obscured regional soft tissues, caused by signal voids and geometric distortion [18].

MRI scanners are designed to have the least distortion at their isocenter, with homogeneity and gradient linearity degrading as the radial distance from the center increases [19]. In this study, the minimum distortion at all the FOVs was found at the isocenter. According to several researchers, the geometric distortion brought on by a gradient nonlinearity is minimal in the magnet's center but becomes more pronounced as one moves outward from the isocenter [12, 20, 21]. The degree of image distortion is caused by the spatial variations that occur during spatial encoding and inhomogeneity of the magnetic field [22]. These distortions are related to the sampling time, which includes the BW and the size of the FOV used. The sampling process proceeds more quickly with a high BW, and there are fewer k-space phase changes between the first and last rows, which reduces image distortions. Similarly, when the FOV is smaller (Table 3), the sampling time decreases and the geometrical distortions decrease [23]. A larger field-of-view (FOV) should be employed to quantify the distortions in accordance with guidelines for MRI scanners used in radiation treatment planning [11]. This is due to the possibility of artifact and geometric distortion when using wider FOVs for these systems [4] as observed in this study.

The total system-related distortions in an MRI simulation of external beam radiotherapy should be less than 2 mm in a 25 cm DSV, according to the American Association of Physicists in Medicine (AAPM) 2021 Report. In planning target volumes with diameters of 2 cm or > 2 cm respectively, it has been reported that a maximum distortion of 1 mm or 1.5 mm is adequate for stereotactic radiosurgery [11]. For FFE acquisitions with a 240 mm FOV, 5 mm slice thickness, and 100 kHz effective bandwidth, the geometrical distortion measured in the frequency encoding direction should be less than 3% [13]. These requirements are also in good agreement with the results in this study. The maximum distortion in the phantom image determined from both low and high bandwidth acquisitions was ≤ 0.67% for all the phantom positions and FOVs. However, distortions measured at 400 mm FOV from the low bandwidth were much greater in the phantom image compared to images acquired with the high bandwidth.

The discrepancy in MFH values between images obtained with and without the use of shimming is shown in Fig. 5. Shimming therefore is one of the reliable methods for reducing magnetic field inhomogeneity and correcting various geometrical distortions [15]. Excellent field homogeneity standards for MRI systems are ideal, but they are insufficient if the MRI system is unable to effectively shim the field when a human body is present. It may be necessary to use effective shimming techniques, such as active shims with high current capacities and higher order terms at high field strengths, in areas of high susceptibilities, such as tissue/air interfaces or metal implants, which will cause significant field inhomogeneities [4].

The average distortion at the 400 mm FOV can also be reduced by increasing the receiver bandwidth but at the cost of SNR. As a result of this, the number of excitations during image acquisition may need to be increased in order to compensate for this decrease in SNR. This might be a workaround for phantom studies, but it might not be feasible for the acquisition of patient images due to the potential increase in scan time and motion artifacts [19]. With increasing field strength and gradient, the SNR and MFH are improved, thereby decreasing image artifacts [2]. This is evident in a study that was conducted with comparable sequence parameters to determine SNR and geometrical accuracy on a 3 T magnet using a balanced FFE sequence. At 450 mm FOV, the SNR was better compared to the values observed in this study [12]. In another study, the MFH measured (i.e., 0.13–0.4 ppm) on a 3 T system was better when compared to that measured on 1.9 T (i.e., 0.6–1.0 ppm) [9]. High-field strength MRI systems may not be able to clearly show geometric distortions brought on by magnetic field inhomogeneity due to the high signal-to-noise ratio (SNR) [24]. Dammann et al. [25] compared geometrical distortion resulting from *Bo* field between a 1.5 and 7 T system and discovered that, for all FFE sequences, the mean distortion remained far below the respective voxel size despite the fact that geometrical distortion typically increases with field strength. By employing a high receiver bandwidth and making sure gradients are properly calibrated, geometric distortions in 7 T systems can be reduced to a clinically relevant level (errors < 1 mm) without experiencing any major susceptibility-related distortions [26].

The main imaging parameter that determines the overall scan time of FFE sequences is the repetition time (*TR*). As a result, imaging with FFE sequences is quicker due to the availability of very short *TR*s (i.e., 20–80 ms).

However, a short *TR* has the downside of reducing the time available for T_1 relaxation [5]. A longer *TR* (113–240 ms) can acquire more slices and enhance SNR [2]. This means that when imaging structures with smaller FOVs (e.g., 200 to 250 mm), it would be more appropriate to use a long *TR* to achieve a high SNR while complementing it with shimming. Also, when imaging with FFE, it is important to ensure that flip angles or angles of excitations between 25° and 45° are used [5, 27]. The net SNR may be lowered and saturation may occur when bigger flip angles (> 50°) are used. Additionally, because the 180-degree pulse is missing from FFE sequences, the effect of static field homogeneity brought on by the variation in different tissues is not compensated for. As a result, the signal (i.e., image contrast of different tissues) decays with T_2^* [5].

According to AAPM Report 100, values of SNR for MRI systems are usually specific. Hence, acceptance criteria for SNR cannot be provided in generic terms such as RF coil, scan conditions, phantom T_1 and T_2 values among others. The baseline or reference values utilized in the ensuing quality assurance program, however, should be the SNR measurements recorded during acceptance testing [13]. For accurate signal and noise measurements, the size of the matrix should be selected to offer a sufficient number of pixels. Typically, a 256 × 256 matrix is recommended [7]. A greater matrix size may reduce SNR while improving measurement precision [28]. Magnetic field homogeneity changes over time, hence quality control (QC) ought to be conducted at commissioning and at least once a year, or after significant maintenance or upgrades that can affect field homogeneity. The commissioning data should be used to create a baseline for the B_0 field homogeneity and its variance. The tolerance should be determined by variations that have been observed over time (i.e., ideally per year) [4]. At the time of this study, no baseline information on image quality tests was available. This is because, no image quality test was performed during the acceptance testing of the MRI scanner, with the exception of measuring insulating resistance, AC/DC magnetic field and vibration, and measuring the effectiveness of shielding on magnet transfer opening, RF door, RF window, and system filter interface. Therefore, the findings of this study could be used as part of benchmarks for future assessments of the whole functionality of MRI scanners for measurements of MFH, SNR, and geometrical distortion.

Study limitations

According to AAPM Report 100, larger phantoms that are at least 35 cm DSV spanning a broader area of space are recommended for evaluating MFH [13]. The smaller DSV (i.e., 15 cm) used in this study might not measure filed homogeneity up to a significant diameter across the bore, thus missing out on field characteristics further away from the isocenter. Also, the gradient fields are assumed to be calibrated accurately for the bandwidth approach. Therefore, unless precise gradient calibrations (across the test FOV) are validated before this technique is utilized to assess MFH, this test is frequently more effective for routine quality control than for acceptance testing [13].

Conclusions

Magnetic field homogeneity is crucial since it has a direct impact on image quality and diagnostic precision during clinical MRI examination. Clear, accurate, and artifact-free images are necessary for precise diagnosis and treatment planning, and a uniform magnetic field is important for obtaining these images. In this study, we have presented a quality control test that may be used as part of routine quality assurance for MRI scanners to optimize magnetic field homogeneity, reduce geometrical distortion, and increase the signal-to-noise ratio using a phantom on a 1.5 T system.

Recommendation

The use of larger DSV phantoms (≥ 35 cm) to investigate the impact of magnetic field homogeneity on image quality across MRI systems with different field strengths, originating from either the same or different manufacturers is highly recommended for comparison purposes and generalization of the findings.

Abbreviations

FFE	Fast field echo
MFH	Magnetic field homogeneity
SNR	Signal-to-noise ratio
FOV	Field of view
GD	Geometrical distortion
MRI	Magnetic resonance imaging
FWHM	Full width at half maximum
ΔBW	Bandwidth difference
DSV	Diameter of spherical volume
ACR	American College of Radiology
AAPM	American Association of Physicists in Medicine

Acknowledgements

The authors would like to thank the following for their support: University of Ghana—Building A New Generation of Academics in Africa (BANGA-Africa), Ethical Review Committee of Ghana Health Service and the University of Ghana Medical Center, Mr. Albert Azantilo, and Mr. George Nunoo of the University of Ghana Medical Center.

Author contributions

ENM conceived the presented idea and gathered the literature. ENM did the write-up of the manuscript. ANM, SI, and IS contributed to the write-up and verified the analytical methods. All authors contributed to the final manuscript.

Funding

No funding was received.

Availability of data and materials
All data generated or analyzed during this study are included in this published article.

Declarations

Ethics approval and consent to participate
Not applicable.

Consent for publication
Not applicable.

Competing interests
The authors declare that they have no competing interests in this section.

Author details
[1]Department of Medical Imaging, University for Development Studies, Tamale, Ghana. [2]Department of Medical Physics, University of Ghana, Accra, Ghana. [3]Radiation Protection Institute (RPI), Ghana Atomic Energy Commission, Accra, Ghana. [4]Radiological and Medical Sciences Research Institute, Ghana Atomic Energy Commission, Accra, Ghana.

Received: 18 April 2023 Accepted: 24 August 2023
Published online: 04 September 2023

References

1. Markl M, Leupold J (2012) Gradient echo imaging. J Magn Reson Imaging 35(6):1274–1289. https://doi.org/10.1002/jmri.23638
2. Pui MH, Fok EC (1995) MR imaging of the brain: comparison of gradient-echo and spin-echo pulse sequences. AJR Am J Roentgenol 165(4):959–962
3. General Electric (2019) The isocenter and the importance of magnet homogeneity. Accessed 30 July 2022. Data Base: https://www.gehealthcare.co.uk/article/the-isocenter-and-the-importance-of-magnet-homogeneity
4. Gach HM, Curcuru AN, Mutic S, Kim T (2020) Bo field homogeneity recommendations, specifications, and measurement units for MRI in radiation therapy. Med Phys 47(9):4101–4114
5. Weishaupt D, Köchli VD, Marincek B, Froehlich JM, Nanz D, Pruessmann KP (2006) How does MRI work?: An introduction to the physics and function of magnetic resonance imaging. Springer, Berlin
6. Bangerter NK, Taylor MD, Tarbox GJ, Palmer AJ, Park DJ (2016) Quantitative techniques for musculoskeletal MRI at 7 Tesla. Quant Imaging Med Surg 6(6):715
7. Price R, Allison J, Clarke G, Dennis M, Hendrick RE, Keener, Masten J, Nessaiver M, Och J, Reeve D (2015) Magnetic resonance imaging QUALITY CONTROL MANUAL. American College of Radiology Committee on Quality Assurance in Magnetic Resonance Imaging. Accessed 16 Aug 2020. Data Base: https://www.acr.org/-/media/ACR/Files/Clinical-Resources/QC-Manuals/MR_QCManual.pdf
8. Ishimori Y, Kawamura H, Monma M (2016) Evaluation of magnetic field homogeneity using in-out signal cycle mapping in gradient recalled echo images of a mixed water/oil phantom as a rough indication for daily quality control. J Biomed Graph Comput 6(2):7–13
9. Chen HH, Boykin RD, Clarke GD, Gao JH, Roby JW III (2006) Routine testing of magnetic field homogeneity on clinical MRI systems. Med Phys 33(11):4299–4306
10. Bakker CJ, Moerland MA, Bhawandien R, Beersma R (1992) Analysis of machine-dependent and object-induced geometric distortion in 2DFT MR imaging. Mag Reson Imaging 10(4):597–608
11. Nousiainen K, Mäkelä T, Peltonen JI (2022) Characterizing geometric distortions of 3D sequences in clinical head MRI. Magn Reson Mater Phys Biol Med 3:1–3
12. Jang JS, Lee HB, Lee KB, Jeon H, Yang HJ (2020) Comparison of the signal-to-noise ratio and the geometric accuracy between conventional-magnetic bore and wide-magnetic bore 3-T magnetic resonance imaging. J Korean Phys Soc 76:59–65
13. Jackson EF, Bronskill MJ, Drost DJ, Och J, Pooley RA, Sobol WT, Clarke GD (2010) Acceptance testing and quality assurance procedures for magnetic resonance imaging facilities. American Association of Physicists in Medicine, pp 20740–3846
14. Gach HM, Curcuru AN, Mutic S, Kim T (2020) B0 field homogeneity recommendations, specifications, and measurement units for MRI in radiation therapy. Med Phys 47(9):4101–4114
15. Sandgren K (2015) Development of a quality assurance strategy for magnetic resonance imaging in radiotherapy. Master's Thesis in Engineering Physics. Umeå University
16. Manson EN, Inkoom S, Mumuni AN (2022) Impact of magnetic field inhomogeneity on the quality of magnetic resonance images and compensation techniques: a review. Rep Med Imaging 8:43–56
17. Keating K, Walsh DO, Grunewald E (2020) The effect of magnetic susceptibility and magnetic field strength on porosity estimates determined from low-field nuclear magnetic resonance. J Appl Geophys 179:104096
18. Onofrio A (2016) Foreign body imaging with MRI. MRI Web Clinic. Accessed on 4 Aug 2023. Database: https://radsource.us/foreign-body-imaging-mri/
19. Walker A, Liney G, Metcalfe P, Holloway L (2014) MRI distortion: considerations for MRI based radiotherapy treatment planning. Australas Phys Eng Sci Med 37(1):103–113
20. Nakazawa H, Komori M, Shibamoto Y, Takikawa Y, Mori Y, Tsugawa T (2014) Geometric accuracy in three-dimensional coordinates of L eksell stereotactic skull frame with wide-bore 1.5-T MRI compared with conventional 1.5-T MRI. J Med Imaging Radiat Oncol 58(5):595–600
21. Karger CP, Höss A, Bendl R, Canda V, Schad L (2006) Accuracy of device-specific 2D and 3D image distortion correction algorithms for magnetic resonance imaging of the head provided by a manufacturer. Phys Med Biol 51(12):N253
22. Koch KM, Rothman DL, de Graaf RA (2009) Optimization of static magnetic field homogeneity in the human and animal brain in vivo. Progress Nucl Mag Reson Spectrosc 54(2):69
23. Wang H, Balter J, Cao Y (2013) Patient-induced susceptibility effect on geometric distortion of clinical brain MRI for radiation treatment planning on a 3T scanner. Phys Med Biol 58(3):465
24. Jao J, Cheng M, Lee H, Ting J, Chen P (2015) Geometric distortion evaluation using a multi-orientated water-phantom at 0.2 T MRI. Bio-Med Mater Eng 26(s1):S1431-8
25. Dammann P, Kraff O, Wrede KH, Özkan N, Orzada S, Mueller OM, Sandalcioglu IE, Sure U, Gizewski ER, Ladd ME, Gasser T (2011) Evaluation of hardware-related geometrical distortion in structural MRI at 7 Tesla for image-guided applications in neurosurgery. Acad Radiol 18(7):910–6
26. Kirby KM, Koons EK, Welker KM, Fagan AJ (2023) Minimizing magnetic resonance image geometric distortion at 7 Tesla for frameless presurgical planning using skin-adhered fiducials. Med Phys 50(2):694–701
27. Brown MA, Semelka RC (2011) MRI: basic principles and applications. Wiley
28. Clarke GD, Chen HH, Roby III JW, Boykin RD. (2008) Inventors; the University of Texas System, assignee. Methods and apparatus for measuring magnetic field homogeneity. United States patent US 7,443,164

Publisher's Note